JOURNAL OF MATERIALS SCIENCE 15 (1980) 1557 – 1567

# The effect of pressure on the growth rate of trans-1, 4-polyisoprene crystals at pressures of 1 bar to 3.5 kbar

C. K. L. DAVIES, M. C. M. CUCARELLA*
*Department of Materials, Queen Mary College, Mile End Road, London E1 4NS, UK*

The growth rates of both low-melting form and high-melting form trans-1, 4-polyisoprene crystals have been measured in thin films by transmission electron microscopy over a range of pressures up to 3.5 kbar. The effect of pressure is to shift the growth rate versus temperature curves to higher temperatures and to cause a continuous decrease in the maximum with increasing pressure. The variation of the crystal growth rate with temperature can be represented, at all pressures, by an equation derived from secondary nucleation theory. The variation of the crystal growth rate with increasing pressure can be largely accounted for by the measured increase in the equilibrium melting temperature of 15 K kbar$^{-1}$ and the calculated increase in the glass transition temperature of 20 K kbar$^{-1}$. The decrease in the maximum growth rate with increasing pressure results from the continuous decrease in $(T_m^0 - T_g)$. It is suggested that crystals of the same form, grow by the same basic mechanism as at atmospheric pressure and that the major effect of pressure is on the melt rather than on the crystals.

## 1. Introduction

Although considerable work has been carried out on the effect of pressure on polymer crystallization (for reviews see [1–4]) much less data is available on the effects on kinetics of crystallization. While crystallization rates can be determined by following the crystallization process as a function of temperature and time at pressure, the measurement of crystal growth rates requires the ability to stop crystallization at a given time while the specimen is under pressure. The crystallization rate at a given temperature was found to increase with pressure for poly (hexam-etilen succinate), but to decrease if crystallization is carried out at a given supercooling [5]. In the case of the co-polymers, poly (ethylene propylene) and poly(ethylene butene) the crystallization rate at a given temperature decreases as a function of pressure [6–8]. Crystal growth rates have been measured at pressures up to 3.5 kbar for cis-1, 4-polyisoprene [9, 10]. The major effect of increasing pressure was reported to be that of increasing the supercooling with increasing pressure for crystallization at a given temperature, as a result of the increase in the equilibrium melting temperature. The growth rate versus temperature curves were therefore displaced to higher temperatures with increasing crystallization pressure. The growth rate maxima increased with pressure up to 1.5 kbar and thereafter remained approximately constant. If the increase in equilibrium melting temperature with increasing pressure is a general phenomena, then whether the crystallization or crystal growth rate at a given temperature, increases or decreases with pressure will depend on the temperature of comparison.

The present work reports crystal growth rate data for trans-1, 4-polyisoprene (TPI) at pressures up to 3.5 kbar. This unsaturated polymer was studied as it is possible to stop crystallization at pressure by a reaction with osmium tetroxide vapour. Crystallization was carried out in thin films of the polymer as it was then possible to study morphology, lamellar thickness and crystal growth

*Present address: Escuela de Ingenleria Metalurgica y ciencia de los Materials, U.C.V. Apartado 51717, Caracas, Venezuela.

0022–2461/80/061557–11$03.10/0 © *1980 Chapman and Hall Ltd.* 

rate simultaneously by transmission electron microscopy. Studies of this type have been carried out on TPI at atmospheric pressure and both the morphology and kinetics of crystallization are well documented [11, 12]. The polymer crystallizes in two forms; low-melting form (LMF) and high-melting form (HMF), with equilibrium melting temperatures of 78 and 87° C [13]. LMF spherulites contain only crystals with an orthorhombic unit cell and HMF spherulites crystals with a monoclinic unit cell [11, 14, 15]. The existence of the two polymorphs allows a study to be made of the effect of pressure on the two crystal growth rates in the same melt.

The effect of pressure on actual melting temperatures and on the equlibrium melting temperatures of both LMF and HMF crystals has been reported previously [4]. All the melting temperatures increase continuously over the range of pressures studied by 15 K kbar$^{-1}$ for both crystal forms. This increase was a direct result of pressure on the thermodynamics of the system and was not a result of lamellar crystal thickening or increase in crystal perfection. The lamellar thickness was measured by both this film transmission electron microscopy and via low-angle X-ray studies [4] over the pressure range 1 bar to 3.0 kbar. It was found that crystals of a given thickness were formed at a given supercooling independent of the pressure of crystallization. At a given crystallization temperature the thickness of the crystals decreased with increasing pressure. "Chain-extended type" crystals were not formed. It was suggested that crystals of the same form grew, at all pressures studied, by the same basic mechanism. The determination of growth rate data was, in part, carried out to investigate this hypothesis and to determine the validity of existing theories of crystal growth over a range of pressures.

## 2. Experimental details

### 2.1. Materials

The trans-1, 4-polyisoprene was prepared by purification of a commercial grade of gutta percha* by solution and reprecipitation [4, 11]. Thin films for transmission electron microscopy, 100 nm thick. were prepared on a water surface from a 1% solution in benzene as reported previously [4, 11]. Some films were strained prior to crystallization using the method devised by Andrews [16]. All films were melted at pressure prior to crystallization. The molecular weight ($\bar{M}_N$) of the melted sample was $3.0 \times 10^4$.

*Supplied by Penfold Golf Ball Ltd., Birmingham, UK.

### 2.2. High-pressure apparatus

The high-pressure system was originally constructed by Edwards and Phillips [10] and was based on a Crawford's design [3]. Details of the modified apparatus are given elsewhere [3]. The pressure is generated by a two-stage intensification of the pressurizing medium, which in the present study was high-purity argon gas. The first stage intensification was carried out by a gas pump, operated via a standard compressed air line. The final pressure was achieved by a high-pressure intensifier operated by means of a compressed air-driven oil pump. The pressure was determined by following the change in resistance of manganin coil with pressure, which was built into the system. The crystallization vessel was operated at pressures up to 3.5 kbar. The crystallization bomb was fitted with a plug which enabled crystallization to be terminated at any time, at pressure, by staining the sample with osmium tetroxide vapour.

### 2.3. Measurement of growth rates

Following crystallization at a given pressure and temperature for a given time, the thin films were examined in a JEM 7 electron microscope operated at 100 kV. HMF and LMF crystals were distinguished by either their respective electron diffraction patterns [14, 15] or by the difference in melting temperatures [4, 13] and by the obvious difference in growth rates [12]. The growth rates were determined by measuring the longest length of a crystal (strained films, Fig. 1a), and the largest diameter of a spherulite (unstrained films, Fig. 1b) after a given crystallization time. The crystal morphology observed showed no significant differences over the pressure range studied.

## 3. Results and discussion

### 3.1. Growth-rate data

The variation of LMF spherulite diameter with time at various crystallization temperatures and at a pressure of 2.0 kbar is shown in Figs. 2 and 3. The growth rate is seen to be constant over the range of times investigated. The data points in Fig. 2 are for temperatures below the growth rate maxima and in Fig. 3 for temperatures above the maxima. The data for HMF spherulites at a pressure of 2.0 kbar are of a similar form as are the data at

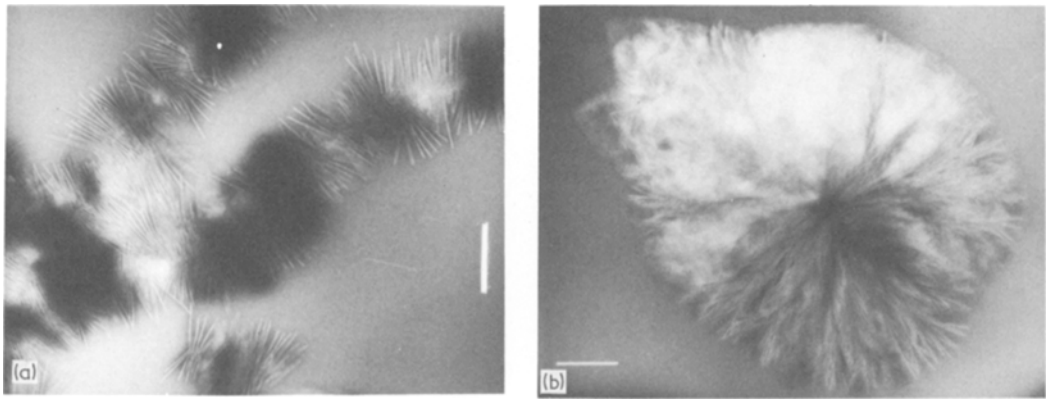


*Figure 1(a)* Electron micrograph showing crystal in a film strained 100% and crystallized at 1 kbar and 60° C for 40 min. Scale bar = 1 μm. (b) Electron micrograph showing a spherulite in a film cyrstallized at 80° C and 2 kbar for 4 h. Scale bar = 1 μm.

all pressures studied. The growth rates at all temperatures and pressures are plotted for LMF crystals in Fig. 4 and for HMF crystals in Fig. 5. The method of calculation of the curves which are drawn through the data points will be given later.

It can be seen in Figs. 4 and 5 that the range of temperatures over which crystallization could be studied was shifted to higher temperatures as the applied pressure increased. The temperature at which the growth rate maxima occurred increased with increasing pressure by approximately 15 K kbar$^{-1}$ for both crystal forms. The crystal growth rate at the maxima decreased continuously with increasing pressure. It is clear that if this trend continues, at higher pressures crystal growth will effectively cease.

At atmospheric pressure it is not normally possible to measure TPI crystal growth rates at or below the growth rate maxima [12, 17–19]. As is common to some other polymers, the rate of crystallization at the maxima is too fast to allow measurement to be made and attempts at quenching through the maxima result in crystallization on cooling at a temperature above the maxima. However, with increasing pressure the

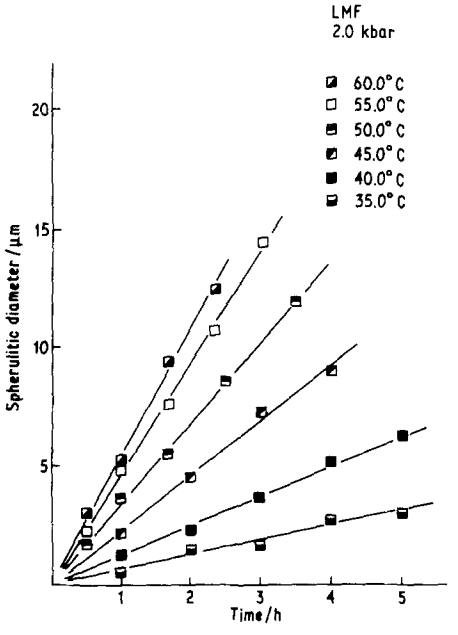


*Figure 2* Variation of LMF TPI spherulite diameter with time at various crystallization temperatures at 2.0 kbar.

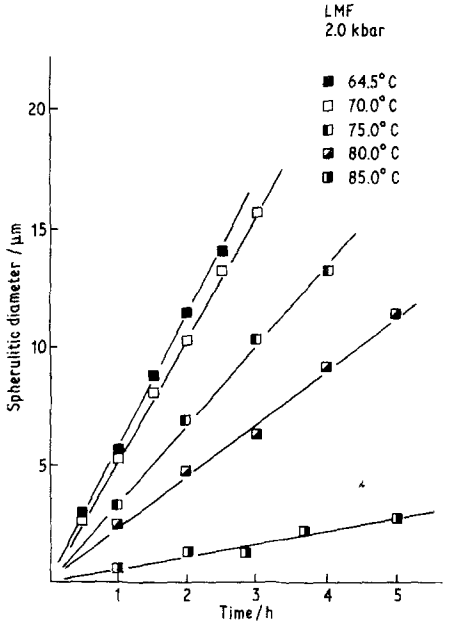


*Figure 3* Variation of LMF TPI spherulite diameter with time at various crystallization temperatures at 2.0 kbar.

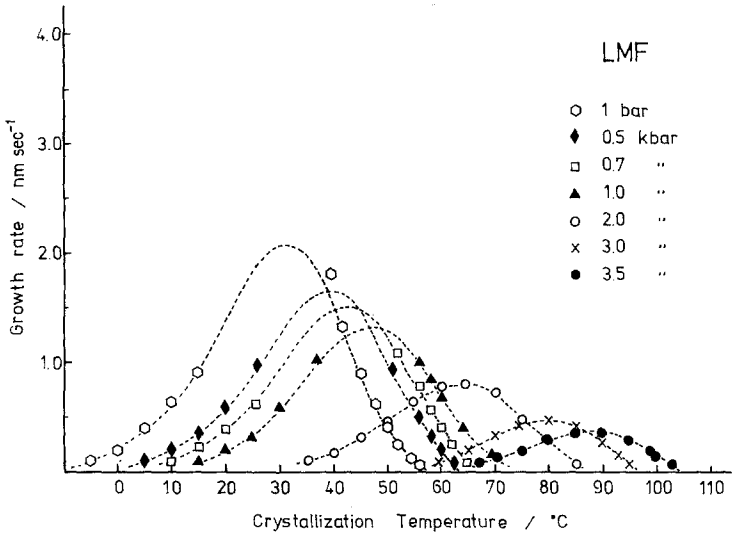


*Figure 4* LMF TPI spherulite growth rate as a function of crystallization temperature for various crystallization pressures.

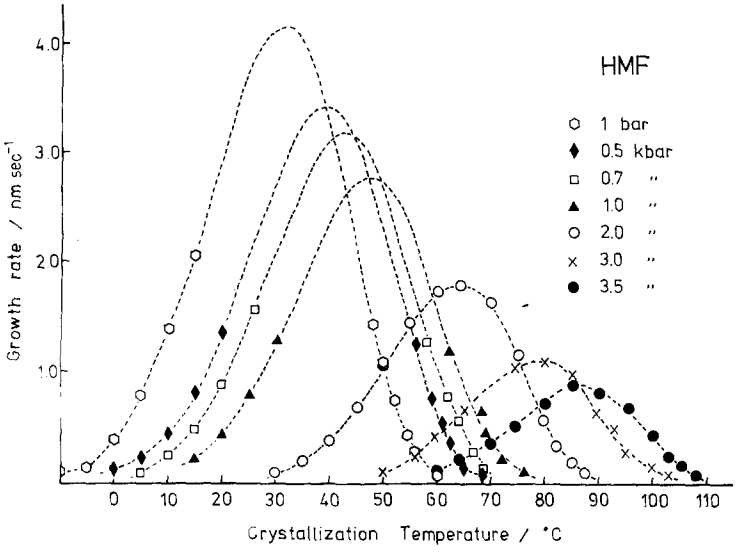


*Figure 5* HMF TPI spherulite growth rate as a function of crystallization temperature for various crystallization pressures.

growth rate at the maxima decreases, to the extent that quenching through the maxima at pressures of 2 kbar and above prevents crystallization occuring. This allows the growth rate to be measured at temperatures below the maxima at these pressures (Figs. 4 and 5). The molten polymer at 100° C and 2 kbar can be quenched to any temperature without immediate crystallization occurring. If the pressure on the sample is now reduced, the growth rate can be measured at a temperature below the growth rate maxima for any pressure below 2 kbar (Figs. 4 and 5). However, it is still not possible to measure the very fast growth rates at the maxima at pressures below 2 kbar.

Both crystal forms were observed at all crystallization pressures. At a given temperature and pressure HMF crystals grew faster than LMF crystals. The value of the maximum growth rate and the range of temperature over which crystallization occurs changes in exactly the same way with increasing pressure for both LMF and HMF crystals (Figs 6 and 7). The maximum growth rate occurs at the same temperature, at any given pressure for both HMF and LMF crystals. The growth rate versus temperature curves remain symetrical about this temperature at all pressures. It would therefore seem that the effect of pressure is primarily on the properties of the melt rather than on the crystal structure or morphology.

Using the previously measured equilibrium melting temperatures [4], the crystal growth rates for HMF and LMF crystals are plotted as a function

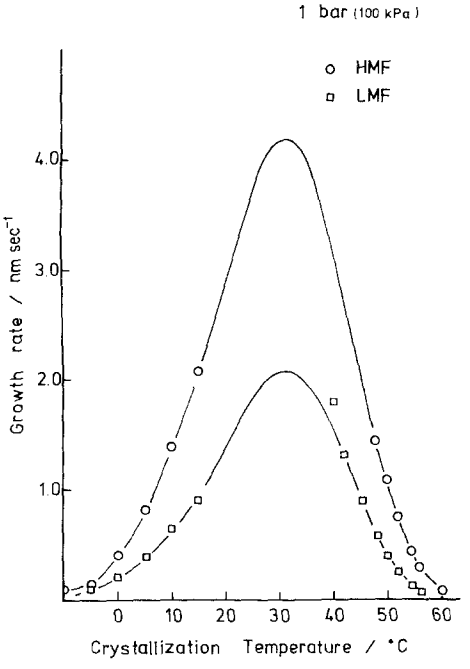


*Figure 6* LMF and HMF TPI spherulite growth rate as a function of crystallization temperature at 1 bar.

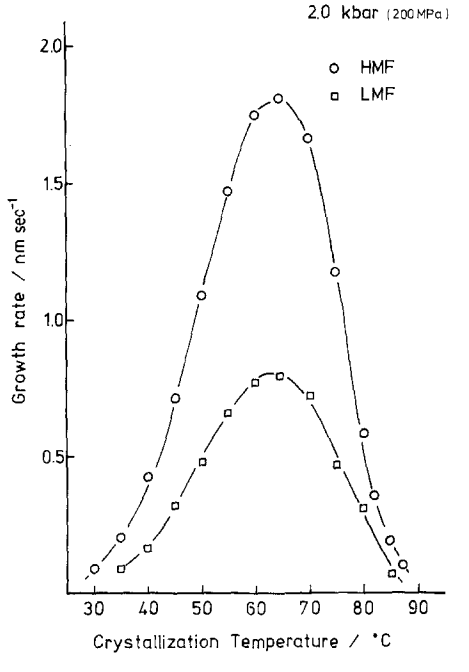


*Figure 7* LMF and HMF TPI spherulite growth rate as a function of crystallization temperature at 2.0 kbar.

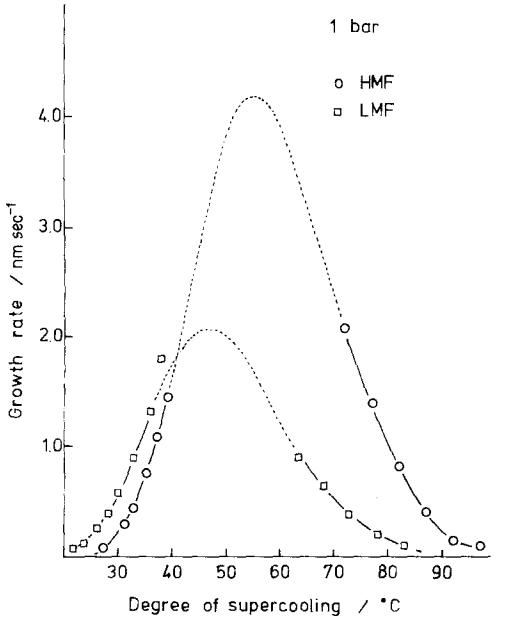


*Figure 8* LMF and HMF TPI spherulite growth rate as a function of degree of supercooling at 1 bar.

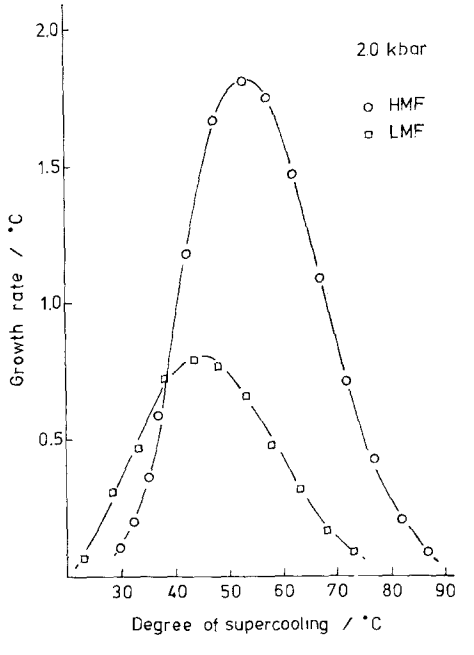


*Figure 9* LMF and HMF TPI spherulite growth rate as a function of degree of supercooling at 2.0 kbar.

of degree of supercooling at pressures of 1 bar and 2 kbar in Figs. 8 and 9. The curves for LMF and HMF crystals cross at a temperature just above the growth rate maxima in the LMF curve at a degree of supercooling of 40° C at all pressures. This is as predicted at atmospheric pressure when only data above the maxima was available [12]. This again suggests that the major effect of pressure is on the melt rather than on the crystal properties. The HMF crystals have faster growth rates than LMF at large supercoolings, while LMF

crystals grow faster than HMF crystals at small supercoolings. This occurs as the available driving force for growth is initially larger for LMF crystals (due to the relatively small surface energies) but increases much more rapidly with increasing supercooling for HMF crystals [4, 12].

At low temperatures, the majority of spherulites observed are of the LMF type. This is clearly not a consequence of relative growth rates as HMF crystals grow faster than LMF crystals at a given temperature and pressure. The maximum nucleation density occurs at approximately the same temperature as the maximum growth rate at all pressures. The nucleation density decreases with increasing pressure in the same way as the growth rate. The nucleation density of the HMF crystals relative to that of the LMF crystals diminished with decreasing crystallization temperature at all pressures. This leads to an increasing preponderance of LMF spherulites at low temperatures. The fact that the nucleation density for both LMF and HMF crystals changes in the same way with increasing pressure again suggest that the primary effect of increasing pressure is on the melt rather than on the structure and properties of the crystals.

## 4. Analysis of crystal growth rate

### 4.1. Growth-rate equation

If crystal growth of chain-folded crystals at a temperature $T$, can be described by a secondary nucleation model [20], the linear growth rate can be represented by an equation of the form

$$G = G_0 \exp\left[-U^*/R(T-T_\infty)\right] \exp\left(-\alpha b\sigma\,\sigma_e/\Delta G_c kT\right). \quad (1)$$

The first exponential is a mobility term and contains the activation energy ($U^*$) for transport of "segments" of molecules to the site of crystallization. $T_\infty$ is a hypothetical temperature where all motion associated with viscous flow ceases, and is somewhat below the glass transition temperature. $R$ is the gas constant.

The second exponential is a driving force term and contains the Gibbs free energy change on crystal formation ($\Delta G_c$) and the work per area to create the fold surfaces ($\sigma_e$) and side surfaces ($\sigma$). The value of $\alpha$ will be 4 if only one nucleus per growth force is formed (regime I) and 2 if multiple nucleation occurs on the growth force (regime 2). $b$ is the thickness of the layer added to the growth face measured in the growth direction and $k$ is the Boltzman constant. The pre-exponential factor $G_0$ contains terms largely insensitive to temperature compared to the exponential terms. It contains the segmental jump frequencies and has dimensions of length per time.

### 4.2. Growth-rate parameters

In order to compare the predictions of Equation 1 with the present growth-rate data it is first necessary to make some estimate of the temperature dependence of the free energy change $\Delta G_c$. At very small supercoolings, if the enthalpy and entropy changes are assumed temperature independent

$$\Delta G_c \simeq \Delta H_c \frac{\Delta T}{T_m^0}, \quad (2)$$

where $\Delta H_c$ is the enthalpy change at $T_m^0$ on crystal formation and $T_m^0$ the equilibrium melting temperature. This estimate is likely to be inaccurate for the present data as $\Delta H_c$ is temperature dependent. At higher supercoolings better estimates are [21, 22]

$$\Delta G_c = \left(\Delta H_c \frac{\Delta T}{T_m^0}\right)\frac{T}{T_m^0} \quad (3)$$

$$\Delta G_c = \left(\Delta H_c \frac{\Delta T}{T_m^0}\right)\left(\frac{2T}{T_m^0 + T}\right). \quad (4)$$

Equations 3 and 4 will both be tried in Equation 1 and the second exponential will be represented as;

$$\exp\left(\frac{-\alpha b\,\sigma\,\sigma_e}{\Delta G_c kT}\right) = \exp-\left[\frac{K_g}{T(\Delta T)F}\right] \quad (5)$$

with

$$K_g = \frac{\alpha\, b\,\sigma\,\sigma_e\, T_m^0}{\Delta H_c K} \quad (6)$$

and

$$F = (T/T_m^0) \text{ or } F = \left(\frac{2T}{T_m^0 - T}\right). \quad (7)$$

Independent measured values of $U^*$ and $T_\infty$ do not exist, partly as it is not clear what "segment" lengths are involved in the thermally activated transport process. $U^*$ and $T_\infty$ can either be considered as ajustable parameters or the term approximated by Williams–Landel–Ferry relation [23]

$$\frac{U^*}{R(T-T_\infty)} = \frac{C_1}{R(C_2 + T - T_g)}, \quad (8)$$

where $T_g$ is the glass transition temperature; $C_1$ and $C_2$ are constants taken to be 17.24 kj mol$^{-1}$ and 51.6° C respectively.

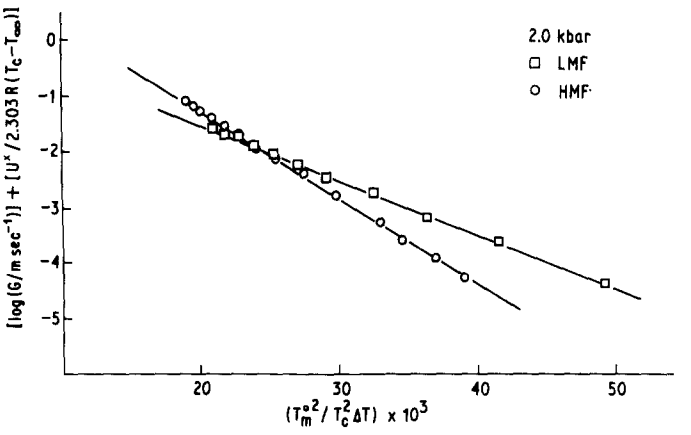


*Figure 10* Regression line, log $G + C_1/2.303R(T_c - T_g + C_2)$ versus $(T_m^0)^2/(T_c)^2\,(T_m^0 - T_c)$ for LMF and HMF crystal grown at 2.0 kbar.

## 4.3. Computing methods

Two computing methods were employed in an attempt to fit the data to Equation 1. In both cases the numerical value of the mobility exponential term must be equal, at a given temperature, for both HMF and LMF crystals as they grow from the same melt.

The first method uses the "universal" WLF constants. The growth rate Equation 1 becomes,

$$\log G = \log G_{0,1} - \frac{C_1}{2.303R(C_2 + T - T_g)} - \frac{K_g T_m^0}{2.303\, T^2\,(\Delta T)} \quad (9)$$

$$\log G = \log G_{0,2} - \frac{C_1}{2.303R(C_2 + T - T_g)} - \frac{K_g (T_m^0 + T)}{4.606\, T^2\,(\Delta T)}, \quad (10)$$

after substitution of Equations 5 and 8 and taking logarithms. Equation 9 uses the first value for $F$ given in Equation 7 and Equation 10 the second value. The two equations were fitted to both the LMF and HMF data. The optimal values for $G_0$ and $K_g$ were determined by a least-mean square analysis of the experimental data. The values of the equilibrium melting temperature are 87 and 78° C, respectively, and increase by approximately 15 K kbar$^{-1}$ [4]. The value of $T_g$ at atmospheric pressure is −60° C [19] but unfortunately no values are available at higher pressures. The least-square analysis was therefore carried out fitting the straight line for different values of $T_g$ and selecting the best fit. The fit corresponded to an increase of $T_g$ of 20 K kbar$^{-1}$. An example of the regression lines used to determine $K_g$ and $G_0$ from Equation 9 and 10 is shown in Fig. 10. The calculated values of $K_g$ and $G_0$ for LMF crystals are given in Table I. It can be seen that the value of $K_g$ remains almost constant with increasing pressure and does not depend strongly on the approximation used for $F$. The correlation factor is also similar for both calculations. The value of $G_0$ also remains almost constant with increasing pressure but is significantly different depending on which approximation for $F$ is used. Equation 10 was used to draw the curves through the data in Figs. 4 and 5 using the calculated values of $T_g$, $G_0$, $K_g$ and the measured values of $T_m^0$. The curves are seen to fit the data well.

TABLE I Fitting of the growth-rate equation using WLF constants. LMF crystals

| $P_c$ (kbar) | $f = T/T_m^0$ | | | $f = \frac{2T}{T_m^0 + T}$ | | |
|---|---|---|---|---|---|---|
| | $K_{g,1} \times 10^{-5}$ ($K^{-2}$) | $G_{0,1}$ (m sec$^{-1}$) | c.c.1 | $K_{g,2}$ ($K^{-2}$) | $G_{0,2}$ (m sec$^{-1}$) | c.c.2 |
| $1 \times 10^{-3}$ | 0.83 | 3.6 | 0.9997 | 0.81 | 1.9 | 0.9997 |
| 0.5 | 0.86 | 3.8 | 0.9998 | 0.84 | 2.1 | 0.9997 |
| 0.7 | 0.86 | 3.7 | 0.9987 | 0.84 | 2.0 | 0.9985 |
| 1.0 | 0.83 | 2.9 | 0.9990 | 0.81 | 1.6 | 0.9992 |
| 2.0 | 0.86 | 2.7 | 0.9990 | 0.84 | 1.6 | 0.9992 |
| 3.0 | 0.91 | 2.8 | 0.9993 | 0.90 | 1.7 | 0.9992 |
| 3.5 | 0.96 | 3.8 | 0.9985 | 0.95 | 2.3 | 0.9983 |

The second method of calculation used a modification of the Susuki and Kovacs method [22]. This method fits the pair of equations derived from Equations 1 and 5.

$$\log G^{\mathrm{HMF}} = \log G_0{}^{\mathrm{HMF}} - \frac{U^*}{2.303R(T-T_\infty)} - \frac{K_g{}^{\mathrm{LMF}}}{2.303\,T(\Delta T)F} \quad (11)$$

and

$$\log G^{\mathrm{LMF}} = \log G_0{}^{\mathrm{LMF}} - \frac{U^*}{2.303R(T-T_\infty)} - \frac{K_g{}^{\mathrm{LMF}}}{2.303\,T(\Delta T)F}, \quad (12)$$

using a maximization of the Pearson correlation coefficient. The method was applied using the two values of $F$ given in Equation 7. $G_0$ and $K_g$ were nominated as dependent variables and $U^*$ and $T_\infty$ were allowed to vary independently. The maximum correlation coefficients for $U^*$ and $T_\infty$ were calculated and then a total maximum for all $U^*$ and $T_\infty$ was found for each crystal form. The product of the maxima for each crystal form was then maximized. From these values, of $U^*$ and $T_\infty$, a simple linear sum of square regression was carried out to determine $G_0$ and $K_g$. Using this procedure the majority of $U^*$ values lay in the range 19 000 to 22 000 J mol$^{-1}$ but at some pressures $U^*$ oscillated critically. This almost certainly occurs due to the lack of data near some growth rate maxima. It was decided to average out the value of $U^*$ for various pressures and to fix this value at 21 700 J mol$^{-1}$ at each pressure. The best value of $T_\infty$ at each pressure was then determined by maximizing the correlation coefficient. The calculated values of $G_0$, $T_\infty$ and $K_g$ are given in Table II. As with the first method, the values of $K_g$ do not change significantly with increasing pressure and they are largely insensitive to the approximation used for $F$ There is, however, a tendency for $K_g$ for HMF crystals to increase at high pressures. $T_\infty$ is found to increase by approximately 20 K kbar$^{-1}$. The value of $G_0$ is largely pressure-independent but tends to increase at the highest pressure.

It is clear that using either computing method the growth-rate data at all pressures can be fitted to Equation 1, with $T_g$ or $T_\infty$ increasing by 20 K kbar$^{-1}$ and using the measured increase of $T_m^0$ of 15 K kbar$^{-1}$. $G_0$ and $K_g$ are largely pressure-independent but tend to increase at the highest pressure.

## 4.4. Surface energies

$K_g$ is given by Equation 6 with $\alpha = 4$ for regime I crystallization and $\alpha = 2$ for regime II crystallization. The calculation of surface energies requires, therefore, knowledge of the basic secondary nucleation growth mechanism. Following the procedure suggested by Hoffman *et al.* [24] and using the calculated values of $K_g$ it was estimated that crystallization took place by a regime II type mechanism at most temperatures. At very low supercoolings an intermediate regime may operate. The calculation of surface energies from the calculated values of $K_g$ using Equation 6 was therefore carried out using $\alpha = 2$, i.e.

$$K_{g(\mathrm{II})} = \frac{2\,b\,\sigma\,\sigma_e\,T_m^0}{k\,\Delta H_c}. \quad (13)$$

This implies that crystal growth takes place by multiple nucleation on the growth face. $\Delta H_c$ is taken to be equal to $\Delta H_m$, the enthalpy change on crystal melting.

To calculate $\sigma\sigma_e$ from Equation 13 requires a knowledge of the variation of $\Delta H_m$ with crystallization pressure. It has been pointed out previously [4] that the $\Delta H_m$ required in this case is that resulting directly from the effect of pressure on the melting of crystals via the Clausius–Clapeyron equation, as no increase in $\Delta H_m$ is anticipated due to crystal thickening or increase in crystal perfection. Unfortunately, no reliable molar volume changes, as a function of pressure, are available and hence it is not possible to estimate the variation in $\Delta H_m$. It is not even possible to guess at the sense of the $\Delta H_m$ change with increasing pressure as both no change, increases and decreases have been observed for various polymer [3, 4]. If $\Delta H_m$ is assumed to be pressure-independent as is effectively observed for branched polyethylene [4, 25], then values of $\sigma\sigma_e$ can be calculated.

The calculated values of $\sigma\sigma_e$ for HMF crystals are given in Table III together with the values of $\sigma_e$ previously determined from the lamellar thickness data [4] and the derived $\sigma$ values. The $K_g$ values agree well with previous determinations from crystallization at atmospheric pressure [12] but the $\sigma\sigma_e$ values differ by a factor of 2 due to the previous assumption of growth by a single nucleus per growth face (regime I). It can be seen that there is a tendency for $\sigma$ to decrease with increasing crystallization pressure with $\sigma_e$ tending to increase.

TABLE II Fitting of the growth-rate equation using $U^* = 21\,685.23$ J mol$^{-1}$* and floating $T_\infty$. HMF and LMF fitted together

| $P_c$ (kbar) | $f = \frac{T}{T_m^0}$ | | | | | | $f = \frac{2T}{T_m^0 + T}$ | | | | | |
|---|---|---|---|---|---|---|---|---|---|---|---|---|
| | $T_\infty$ (K) | c.c.3 | HMF $G_{0,3}$ (m sec$^{-1}$) | LMF $G_{0,3}$ (m sec$^{-1}$) | HMF $K_{g,3} \times 10^{-5}$ (K$^2$) | LMF $K_{g,3} \times 10^{-5}$ (K$^2$) | $T_\infty$ (K) | c.c.4 | HMF $G_{0,4}$ (m sec$^{-1}$) | LMF $G_{0,4}$ (m sec$^{-1}$) | HMF $K_{g,4} \times 10^{-5}$ (K$^2$) | LMF $K_{g,4} \times 10^{-5}$ (K$^2$) |
| $1 \times 10^{-3}$ | 149.0 | 0.9988 | 758 | 48 | 1.31 | 0.87 | 151.1 | 0.9988 | 421 | 39 | 1.30 | 0.87 |
| 0.5 | 158.0 | 0.9988 | 623 | 42 | 1.32 | 0.89 | 159.9 | 0.9989 | 355 | 33 | 1.30 | 0.89 |
| 0.7 | 163.0 | 0.9986 | 656 | 51 | 1.31 | 0.90 | 163.6 | 0.9987 | 361 | 38 | 1.29 | 0.90 |
| 1.0 | 162.0 | 0.9983 | 426 | 23 | 1.31 | 0.84 | 168.2 | 0.9983 | 242 | 18 | 1.29 | 0.84 |
| 2.0 | 187.0 | 0.9988 | 645 | 23 | 1.43 | 0.87 | 188.7 | 0.9988 | 397 | 20 | 1.42 | 0.87 |
| 3.0 | 209.0 | 0.9966 | 895 | 38 | 1.48 | 0.95 | 210.6 | 0.9968 | 597 | 33 | 1.48 | 0.96 |
| 3.5 | 223.0 | 0.9986 | 4154 | 138 | 1.66 | 1.06 | 223.8 | 0.9987 | 2180 | 99 | 1.64 | 1.05 |

*Average of the best fit values floating all parameters using a variation of Susuki and Kovacs method

TABLE III Surface energies for HMF crystals

| $P_c$ (kbar) | $\frac{\sigma\sigma_e}{\Delta H_m} \times 10^{12}$ ($m^{-1}$) | $\sigma\sigma_e^* \times 10^6$ ($J^2\ m^{-4}$) | $\sigma_e^\dagger \times 10^3$ ($J\ m^{-2}$) | $\sigma \times 10^3$ ($J\ m^{-1}$) |
|---|---|---|---|---|
| $1 \times 10^{-3}$ | 5.05 | 1000.7 | 56.9 | 17.6 |
| 0.5 | 4.95 | 980.3 | 61.4 | 16.0 |
| 0.7 | 4.88 | 966.2 | – | – |
| 1.0 | 4.81 | 953.3 | 59.9 | 15.9 |
| 2.0 | 5.10 | 1009.0 | 69.9 | 14.3 |
| 3.0 | 5.11 | 1012.7 | 71.8 | 14.1 |
| 3.5 | 5.56 | 1101.7 | – | – |

*Calculated considering $\Delta H_m$ pressure-independent.
†Obtained from lamellar thickness data.

## 5. Conclusions

The crystal growth rate versus temperature curves for both LMF and HMF TPI crystals are of the same form at all pressures studied. Crystallization at increasing pressure shifted the curves to higher temperature ranges and the maximum crystal growth rate was observed to decrease continuously with increasing pressure. The growth rates of both LMF and HMF TPI crystals vary with pressure in exactly the same way over the pressure range studied.

The variation of the crystal growth rate with temperature can be represented at all pressures by an equation derived from the Lauritzen and Hoffman Kinetic theory [20]. The variation of the crystal growth rate with increasing pressure can be largely accounted for by the measured increase in $T_m^0$ of 15 K $kbar^{-1}$ and the calculated increase in $T_g$ of 20 K $kbar^{-1}$. The increase in both these parameters occurs directly as a result of pressure on the thermodynamics of the system and not indirectly as a result of crystal thickening or increase in crystal perfection. It is suggested that over the pressure range studied, crystals of the same form grow by the same mechanism as at atmospheric pressure. The major effect of pressure is on the melt rather than on the crystals.

The decrease in the maximum growth rate with increasing pressure results from the continuous decrease in $(T_m^0 - T_g)$. If this decrease continues, crystal growth by the low-pressure mechanism will effectively cease at some finite pressure. If chain-extended crystals are to form at higher pressures, in a finite time, then growth must occur by a different mechanism. This mechanism would require a much more efficient system of transport of molecules to the crystal and may involve ordering of groups of molecules in the melt prior to the formation of crystals with definite boundaries.


## Acknowledgements

The authors would like to thank the Science Reasearch Council for financial support for this work. One of the authors, Martha C.M. Cucarella would like to thank the Consejo de Desarrollo Cientifico y Humanistico of Venezuela for the maintenance grant that enabled this work to be carried out, and to thank the Department of Metallurgy and Materials Science of the Universidad Central de Venezuela for leave of absence. The authors would also like to thank Professor E. H. Andrews for helpful discussion and Dr D. A. Tod for help in apparatus design, computing work and general discussion throughout this work.


## References


1. B. WUNDERLICH, *Marcomol. Phys.* **1** (1973) 217.
2. D. C. BASSETT, *Polymer* **17** (1976) 460.
3. M. C. M. CUCARELLA, Ph.D. Thesis, University of London (1978).
4. C. K. L. DAVIES and M. C. M. CUCARELLA, *J. Mater. Sci.* **15** (1980) 1547.
5. F. ASMUSSEN, W. SCHWINAN and K. UEBERREITER, *Kolloid-Z.Z. Polymere* **250** (1972) 506.
6. D. BODILY and B. WUNDERLICH, *J. Polymer Sci. A2* **4** (1966) 25.
7. T. ARAKAWA and B. WUNDERLICH, *ibid A2* **4** (1966) 53.
8. J. DAVIDSON and B. WUNDERLICH, *ibid* **7** (1969) 377.
9. P. J. PHILLIPS and E. H. ANDREWS, *ibid* **B10** (1972) 321.
10. P. J. PHILLIPS and B. C. EDWARDS, *ibid* **A13** (1974) 1819.
11. C. K. L. DAVIES and ONG ENG LONG, *J. Mater. Sci.* **12** (1977) 2165.
12. *Idem, ibid.* **14** (1979) 2529.
13. E. G. LOVERING and D. C. WOODEN, *J. Polymer Sci. A2* **9** (1971) 175.
14. C. W. BUNN, *Proc. Roy. Soc.* **A180** (1942) 40.
15. D. FISCHER, *Proc. Phys. Soc. A* **66** (1953) 7.
16. E. H. ANDREWS, *Proc. Roy. Soc.* **A227** (1964) 562.
17. E. FISCHER and J. F. HENDERSON, *J. Polymer Sci. A-2* **5** (1967) 37.
18. E. G. LOVERING, IUPAC Sumposium on Macromolecules, Toronto (1968) Paper A6:16.
19. *Idem, J. Polymer Sci. A-2* **8** (1970) 747. 747.
20. J. I. LAURITZEN JR and J. D. HOFFMAN, *J. Appl. Phys.* **44** (1973) 4340.
21. J. D. HOFFMAN and J. J. WEEKS, *J. Res. Nat. Bur. Stand.* **66A** (1962) 13.
22. T. SUZUKI and A. J. KOVACS, *Polymer J.* **1** (1976)

82.
23. M. L. WILLIAMS, R. F. LANDEL and J. D. FERREY, *J. Amer. Chem. Soc.* 77 (1955) 3701.
24. J. D. HOFFMAN, G. T. DAVIES and J. LAURITZEN JR, "Treatise on Solid State Chemistry", Vol. 3 (Plenum Press, New York 1976).
25. S. MATSUSKA, *J. Polymer Sci.* 57 (1962) 569.

Received 13 September and accepted 13 November 1979.